PERGAMON

International Journal of Solids and Structures 38 (2001) 9179–9199

INTERNATIONAL JOURNAL OF SOLIDS and STRUCTURES

www.elsevier.com/locate/ijsolstr

An efficient coupled theory for multilayered beams with embedded piezoelectric sensory and active layers

Santosh Kapuria *

ETD(Analysis), EIH-8th Floor, Engineers India Limited, 1, Bhikajee Cama Place, New Delhi 110066, India

Received 13 October 2000; accepted 27 March 2001

Abstract

An efficient coupled electromechanical model is developed for multilayered composite beams with embedded or surface bonded piezoelectric laminae subjected to static electromechanical excitation. The model combines third order zigzag approximations for the displacement field with a layerwise representation of the electric field. Interfacial continuity of the inplane displacement and the transverse shear stress and traction free conditions on the top and bottom surfaces are ensured under general electromechanical loading situation. The model allows for a non-uniform variation of transverse displacement in the piezoelectric layers caused by the electric field induced normal transverse strain. The theory has the same number of primary variables as first order theory and hence the computational cost is independent of the number of layers in the laminate. The governing equations of stress and charge equilibrium and the variationally consistent boundary conditions are derived from the principle of virtual work. To illustrate the accuracy, applicability and robustness of the theory, an analytical solution is obtained for hybrid beams with simply supported ends. Present results for simply supported hybrid beams with sensory and actuated piezoelectric layers are compared with the exact three dimensional solution and uncoupled first order theory solution. The present results show significant improvement over the first order solution and compare very well with the exact solution for both thin and thick piezoelectric laminated beams. Capability of the developed theory to model sensory, active and combined response of smart composite beams with general laminate configurations has been demonstrated through additional numerical examples. Feasibility of controlling deflection by applying appropriate actuation potential has been illustrated.

Keywords: Smart composite beam; Coupled theory; Zigzag displacement; Layerwise potential; Piezoelectric

1. Introduction

Hybrid beams and plates made up of an elastic multilayered substrate with embedded or surface-bonded piezoelectric sensory and actuator layers constitute an important class of smart structures which have received enormous research attention in recent years. Due to inhomogeneities in the mechanical properties across the thickness and presence of electric heterogeneity caused by the embedded piezoelectric layers,

* Tel.: +91-011-610-2121, ext.: 2678/2381; fax: +91-011-619-2693.
E-mail address: s_kapuria@hotmail.com (S. Kapuria).

0020-7683/01/$ - see front matter
PII: S0020-7683(01)00112-3

analysis of these structures requires appropriate electromechanical modelling. Ideally, an accurate response of these hybrid structures, in the domain of linear piezoelasticity, can be obtained by solving the three dimensional (3D) coupled field equations subject to the exact satisfaction of the boundary and interlaminar continuity conditions. 3D analytical solutions have been presented for the piezoelectric response of simply supported infinite hybrid flat panels (Ray et al., 1992, 1993; Brooks and Heyliger, 1994; Zhou and Tiersten, 1994; Kapuria et al., 1997a) and rectangular plates (Heyliger, 1994; Lee and Jiang, 1996). Finite element models for piezoelectric plate structures based on the 3D theory have also been presented (see e.g. Naillon et al., 1983; Ha et al., 1992). The exact 3D analytical solutions are, however, available only for some regular shapes with specific boundary conditions. On the other hand, its finite element implementation typically results in large problem size requiring high computational effort and costs for practical applications and often becomes computationally intractable particularly for dynamics and control problems. It is to overcome these drawbacks of the 3D theory that approximations are made about the through-the-thickness distributions of the field variables to arrive at a 2D model for analysis of multilayered piezoelectric structures. Several 2D theories (1D for beams) for hybrid laminated beams and plates have been reported in the literature. Early works were based on the classical laminate theory (CLT) approximation for the mechanical field without considering the coupling between the mechanical and the electric fields (Tzou, 1989; Lee and Moon, 1989; Lee, 1990; Crawley and Lazarus, 1991). The limitation of CLT of not including the shear deformation effect was addressed soon by using first order shear deformation theory (FSDT) (see e.g. Jonnalagadda et al., 1994; Kapuria et al., 1997b) and refined third order theory of Reddy (1984) (see e.g. Pai et al., 1993; Peng et al., 1998) for the analysis of hybrid beams and plates under electromechanical loading. These uncoupled 2D theories ignore constitutive equations for the electric displacements as well as the equation of equilibrium for electrostatic charges and treat the electric field as an external loading through the induced piezoelectric strain in the constitutive equation of stresses. This approach results in inferior solutions for smart structures with embedded piezoelectric sensors and actuators with multiple voltage inputs and/or sensor outputs. Huang and Wu (1996) have presented a FSDT solution including electromechanical coupling for hybrid multilayered piezoelectric plates taking a cubic variation of the electric potential across the laminate thickness. Mitchell and Reddy (1995) have presented a coupled hybrid theory for piezoelectric composite plates based on the refined third order approximation for the displacement field and layerwise approximation for the potential field. The equivalent single layer (ESL) approximations used in the above works for the displacement field suffer from the common drawback that they do not account for the so called zigzag effect in the distribution of inplane displacements across the thickness and do not satisfy the shear stress continuity conditions at the interfaces between adjacent layers. These limitations lead to inaccurate results for thick laminates and laminates with strong inhomogeneities across the thickness. In order to overcome the drawbacks of the ESL theories, discrete layer theories (DLTs) based on layerwise approximations for the displacements have been developed for elastic laminated beams with induced actuation strain by Robins and Reddy (1991). This work has latter been extended by Saravanos and Heyliger (1995), Heyliger et al. (1994) and Saravanos et al. (1997) for coupled layerwise analysis of piezoelectric composite beams and plates. The DLTs have been shown to yield very accurate results for both thin and thick laminates, but they are quite cumbersome and expensive for practical problems because the number of unknowns depend on the number layers in the laminate. To overcome this disadvantage in the case of elastic analysis, various zigzag theories have been proposed for describing the deformations of elastic multilayered composite plates under mechanical loading. These theories retain the zigzag form of distribution of the inplane displacements across the laminate thickness as in the DLTs, but use the shear stress continuity conditions at the interfaces to make the number of unknowns independent of the number of layers as in ESL theories. Among these theories, the third order zigzag theory proposed by Cho and Parmerter (1993, 1994) and Shu and Sun (1994) were shown to be both efficient and accurate in predicting the global as well as through-the-thickness behaviour of thin and thick multilayered plates under mechanical loading. In this theory, the inplane displacement field is taken as a combination of a layerwise

linear (zigzag) variation and a global cubic variation across the thickness. Transverse normal strains are neglected.

The objective of the present work is to develop an efficient coupled electromechanical 1D model for the static analysis of thin and thick multilayered composite beams with embedded or surface bonded sensory and actuator layers. The displacement field approximations of the third order zigzag theory described above are combined with a layerwise approximation for the electric potential so as to achieve the accuracy and robustness of a coupled DLT while preserving the computational advantage of an ESL theory for the mechanical field part. The transverse displacement field is obtained by superimposing a constant deflection with a layerwise variation accounting for the piezoelectric transverse normal strain due to the electric potential. This description allows for the non-uniform distribution of deflection across the piezoelectric layers. Such a variation can be captured in a DLT only if the transverse displacement is also taken as piecewise linear, which makes it even more cumbersome and computationally expensive. The inplane displacement field is obtained by superimposing a layerwise contribution from the electric field intensity along the axial direction on a third order zigzag variation. The conditions of continuity of the inplane displacement and the transverse shear stress at each layer interface and zero shear stress at the top and bottom surfaces of the laminate are enforced under general electromechanical loading situation. It reduces the number of unknowns for the displacement field to three, which is the same as in FSDT. The governing equilibrium equations and variationally consistent boundary conditions for the developed 1D model are derived from the principle of virtual work. To illustrate the model, analytical solution is obtained for the coupled piezoelectric response of a simply supported hybrid beam. The accuracy of the theory is assessed by comparison with the exact 3D piezoelastic solution and uncoupled FSDT solution. Additional results are presented to demonstrate the capability of the developed theory to model sensory, active as well as combined response of smart composite beams with general laminate configurations.

2. Formulation of theory

2.1. Geometry of the hybrid beam

Consider a hybrid beam of solid cross-section of width b and thickness h, consisting of L orthotropic layers with their principal material axis along the fibres at an arbitrary angle to the Cartesian coordinate axis-x along its length. The geometry of the beam is shown in Fig. 1. Some of the layers can be piezoelectric with class mm2 symmetry and poling along the thickness axis-z. The origin of the coordinate system (x, z) is taken at the middle surface of the beam. The integer k denotes the layer number which starts from the bottom of the laminate. The distance from the reference plane to the bottom surface of the kth layer is denoted by z_{k-1}. Each layer is perfectly bonded to its adjacent plies.

2.2. Constitutive equations

For a piezoelectric continuum which exhibits class mm2 symmetry with respect to principal material axes x_1, x_2, $x_3(=z)$ and is polarised along direction z, the constitutive equations referring to the orthogonal coordinate system (x, y, z) are given by (Auld, 1973; Tzou and Bao, 1995)

$$\varepsilon = \bar{S}\sigma + \bar{d}^{\mathrm{T}}E, \quad D = \bar{d}\sigma + \bar{\epsilon}E, \tag{1}$$

where the superscript T denotes matrix transpose. The components of stress σ, engineering strain ε, electric field E and electric displacement D are given by

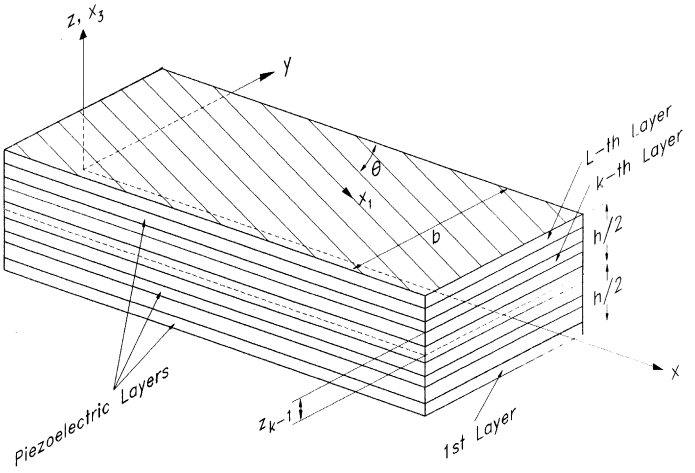

Fig. 1. Geometry of the hybrid beam.

$$\sigma = [\,\sigma_x \quad \sigma_y \quad \sigma_z \quad \tau_{yz} \quad \tau_{zx} \quad \tau_{xy}\,]^{\mathrm{T}}, \quad E = [\,E_x \quad E_y \quad E_z\,]^{\mathrm{T}}, \quad \varepsilon = [\,\varepsilon_x \quad \varepsilon_y \quad \varepsilon_z \quad \gamma_{yz} \quad \gamma_{zx} \quad \gamma_{xy}\,]^{\mathrm{T}},$$
$$D = [\,D_x \quad D_y \quad D_z\,]^{\mathrm{T}}.$$

$\bar{S}$, $\bar{d}$, $\bar{\epsilon}$ are respectively the matrices of transformed compliance coefficients, piezoelectric strain constants and constant stress dielectric constants with

$$\bar{S} = \begin{bmatrix} \bar{S}_{11} & \bar{S}_{12} & \bar{S}_{13} & 0 & 0 & \bar{S}_{16} \\ \bar{S}_{12} & \bar{S}_{22} & \bar{S}_{23} & 0 & 0 & \bar{S}_{26} \\ \bar{S}_{13} & \bar{S}_{23} & \bar{S}_{33} & 0 & 0 & \bar{S}_{36} \\ 0 & 0 & 0 & \bar{S}_{44} & \bar{S}_{45} & 0 \\ 0 & 0 & 0 & \bar{S}_{45} & \bar{S}_{55} & 0 \\ \bar{S}_{16} & \bar{S}_{26} & \bar{S}_{36} & 0 & 0 & \bar{S}_{66} \end{bmatrix}, \quad \bar{d}^{\mathrm{T}} = \begin{bmatrix} 0 & 0 & \bar{d}_{31} \\ 0 & 0 & \bar{d}_{32} \\ 0 & 0 & \bar{d}_{33} \\ \bar{d}_{14} & \bar{d}_{24} & 0 \\ \bar{d}_{15} & \bar{d}_{25} & 0 \\ 0 & 0 & \bar{d}_{36} \end{bmatrix}, \quad \bar{\epsilon} = \begin{bmatrix} \bar{\epsilon}_{11} & \bar{\epsilon}_{12} & 0 \\ \bar{\epsilon}_{12} & \bar{\epsilon}_{22} & 0 \\ 0 & 0 & \bar{\epsilon}_{33} \end{bmatrix}. \tag{2}$$

For a beam with small width, the following assumptions are made:

$$\sigma_z \simeq 0, \quad \sigma_y \simeq 0, \quad \tau_{yz} \simeq 0, \quad \tau_{xy} \simeq 0, \quad E_y \simeq 0. \tag{3}$$

On use of Eq. (3), the constitutive relations in Eq. (1) reduce to

$$\begin{bmatrix} \sigma_x \\ \tau_{zx} \end{bmatrix} = \begin{bmatrix} \bar{Q}_{11} & 0 \\ 0 & \bar{Q}_{55} \end{bmatrix} \begin{bmatrix} \varepsilon_x \\ \gamma_{zx} \end{bmatrix} - \begin{bmatrix} 0 & \bar{e}_{31} \\ \bar{e}_{15} & 0 \end{bmatrix} \begin{bmatrix} E_x \\ E_z \end{bmatrix}$$
$$\begin{bmatrix} D_x \\ D_z \end{bmatrix} = \begin{bmatrix} 0 & \bar{e}_{15} \\ \bar{e}_{31} & 0 \end{bmatrix} \begin{bmatrix} \varepsilon_x \\ \gamma_{zx} \end{bmatrix} + \begin{bmatrix} \bar{\eta}_{11} & 0 \\ 0 & \bar{\eta}_{33} \end{bmatrix} \begin{bmatrix} E_x \\ E_z \end{bmatrix} \tag{4}$$

with $\bar{Q}_{ij} = 1/\bar{S}_{ij}$, $\bar{e}_{31} = \bar{d}_{31}\bar{Q}_{11}$, $\bar{e}_{15} = \bar{d}_{15}\bar{Q}_{55}$, $\bar{\eta}_{11} = \bar{\epsilon}_{11} - \bar{d}_{15}\bar{e}_{15}$, $\bar{\eta}_{33} = \bar{\epsilon}_{33} - \bar{d}_{31}\bar{e}_{31}$. It may be noted here that, unlike most other studies, E_x is not considered zero in the present formulation, since it is an electric field induced by the piezoelectric coupling. This field may also be present due to non-uniform distribution of the applied electric potential along the length of the beam.

2.3. Displacements and potential field

The proposed 1D beam model combines a third order zigzag approximation for the inplane displacement u through the thickness of the laminate with a layerwise approximation for the electric potential ϕ such that the continuity of the transverse shear stress at the interfaces between adjacent layers is satisfied in presence of the electromechanical field. The transverse displacement field w is obtained by superimposing a constant field across the thickness with a layerwise contribution that accounts for the piezoelectric out-of-plane normal strain induced by the electric potential. Accordingly, the displacement and the potential fields are assumed in the following form:

$$u(x,z) = u_k(x) - zw_0(x)_{,x} + z\psi_k(x) + z^2\xi(x) + z^3\eta(x) + \bar{a}^k \sum_{j=1}^{N} f^j(z)\phi^j_{,x}, \tag{5a}$$

$$w(x,z) = w_0(x) - \bar{d}^k_{33} \sum_{j=1}^{N} \Psi^j(z)\phi^j, \quad \phi(x,z) = \sum_{j=1}^{N} \Psi^j(z)\phi^j(x) \tag{5b}$$

with $\bar{a}^k = \bar{d}^k_{33} - \bar{e}^k_{15}/\bar{Q}^k_{55}$ and $f^j(z) = \int_0^z \Psi^j(z)\,\mathrm{d}z$. Here a subscript comma denotes differentiation. u_k and ψ_k denote displacement and rotation variables of the kth layer. N is the number of points z^j across the laminate thickness for describing the variation of the potential field in the thickness direction. ϕ^j are the electric potentials at points z^j and $\Psi^j(z)$ are the interpolation functions which are taken as linear in this work.

The strain–displacement and electric field–potential relations are

$$\varepsilon_x = u_{,x}, \quad \varepsilon_z = w_{,z}, \quad \gamma_{zx} = u_{,z} + w_{,x}, \quad \varepsilon_y = \gamma_{yz} = \gamma_{xy} = 0; \quad E_x = -\phi_{,x}, \quad E_z = -\phi_{,z}, \quad E_y = 0. \tag{6}$$

Using Eqs. (4)–(6), transverse shear strain γ_{zx} and stress τ_{zx} are obtained as

$$\gamma_{zx} = \psi_k + 2z\xi + 3z^2\eta - \bar{e}^k_{15}/\bar{Q}^k_{55} \sum_{j=1}^{N} \Psi^j(z)\phi^j_{,x}, \quad \tau_{zx} = \bar{Q}^k_{55}[\psi_k + 2z\xi + 3z^2\eta]. \tag{7}$$

The functions u_k, ψ_k, ξ and η are determined using the following conditions:

1. The top and bottom surfaces of the beam are traction free i.e. $\tau_{zx}|_{z=\pm h/2} = 0$. Using Eq. (7), it yields

$$\xi = (\psi_1 - \psi_L)/2h, \quad \eta = -2(\psi_1 + \psi_L)/3h^2. \tag{8}$$

2. The shear stress is continuous across each layer interface. Thus, from Eq. (7), we have, at the interface between the $(i-1)$th and the ith layers $(i = 2, \ldots, L)$,

$$\begin{aligned} &\bar{Q}^i_{55}[\psi_i + 2z_{i-1}\xi + 3z^2_{i-1}\eta] = \bar{Q}^{i-1}_{55}[\psi_{i-1} + 2z_{i-1}\xi + 3z^2_{i-1}\eta] \quad \text{or} \\ &\bar{Q}^i_{55}[\psi_i + 2z_i\xi + 3z^2_i\eta] = \bar{Q}^{i-1}_{55}[\psi_{i-1} + 2z_{i-1}\xi + 3z^2_{i-1}\eta] + \bar{Q}^i_{55}[2(z_i - z_{i-1})\xi + 3(z^2_i - z^2_{i-1})\eta] \end{aligned} \tag{9}$$

Applying the above relation recursively from $i = 2$ to k and making use of the traction free condition at the bottom surface, $\tau_{zx}|_{z=-h/2} = \bar{Q}^1_{55}[\psi_1 + 2z_0\xi + 3z^2_0\eta] = 0$, we obtain

$$\bar{Q}^k_{55}[\psi_k + 2z_k\xi + 3z^2_k\eta] = 2C^k_1\xi + 6C^k_2\eta, \tag{10}$$

where $C^k_1 = \sum_{i=1}^{k} \bar{Q}^i_{55}(z_i - z_{i-1})$ and $C^k_2 = \sum_{i=1}^{k} \bar{Q}^i_{55}(z^2_i - z^2_{i-1})/2$. Substitution of the traction free condition on the top surface, $\tau_{zx}|_{z=h/2} = \bar{Q}^L_{55}[\psi_L + 2z_L\xi + 3z^2_L\eta] = 0$, into Eq. (10) for $k = L$ yields

$$C^L_1\xi + 3C^L_2\eta = 0,$$

which is used to eliminate ψ_L from Eq. (8), giving

$$\xi = R_3\psi_1, \quad \eta = R_4\psi_1 \tag{11a}$$

with $R_3 = 4C_2^L/h(hC_1^L + 4C_2^L)$, $R_4 = -4C_1^L/3h(hC_1^L + 4C_2^L)$. Substitution of Eq. (11a) into Eq. (10) yields

$$\psi_k = R_2^k\psi_1, \tag{11b}$$

where $R_2^k = 2(C_1^k/\bar{Q}_{55}^k - z_k)R_3 + 3(2C_2^k/\bar{Q}_{55}^k - z_k^2)R_4$.

3. The displacement u is continuous across each layer interface. Using Eq. (5a), it yields, for the interface between the $(i-1)$th and the ith layers,

$$u_i = u_{i-1} + z_{i-1}(\psi_{i-1} - \psi_i) + (\bar{a}^{i-1} - \bar{a}^i)\sum_{j=1}^{N} f^j(z_{i-1})\phi_{,x}^j, \quad i = 2, \ldots, L. \tag{12}$$

Substituting the expression for ψ_k from Eq. (11b) into Eq. (12) and applying the resulting recursive relation to each interface from $i = 2$ to k, the following expression is obtained for u_k:

$$u_k = u_1 + \sum_{i=2}^{k} z_{i-1}(R_2^{i-1} - R_2^i)\psi_1 + \sum_{i=2}^{k}(\bar{a}^{i-1} - \bar{a}^i)\sum_{j=1}^{N} f^j(z_{i-1})\phi_{,x}^j. \tag{13}$$

Considering that the mid-surface $(z = 0)$ of the beam lies in the k_0th layer, denoting the mid-surface displacement as $u(x, 0) = u_0(x)$ and substituting the same in Eqs. (5a) and (13), the latter equation can be expressed as

$$u_k = u_0 + R_1^k\psi_1 + \sum_{j=1}^{N} R_0^{kj}\phi_{,x}^j, \tag{14}$$

where

$$R_1^k = \sum_{i=2}^{k} z_{i-1}(R_2^{i-1} - R_2^i) - \sum_{i=2}^{k_0} z_{i-1}(R_2^{i-1} - R_2^i), \quad R_0^{kj} = \sum_{i=2}^{k}(\bar{a}^{i-1} - \bar{a}^i)f^j(z_{i-1}) - \sum_{i=2}^{k_0}(\bar{a}^{i-1} - \bar{a}^i)f^j(z_{i-1}).$$

Finally, substitution of Eqs. (11a), (11b) and (14) into Eq. (5a) yields the following expression for u:

$$u = u_0 - zw_{0,x} + R_k(z)\psi_1 + \sum_{j=1}^{N} F_k^j(z)\phi_{,x}^j, \tag{15}$$

where $R_k(z) = R_1^k + zR_2^k + z^2R_3 + z^3R_4$, $F_k^j(z) = \bar{a}^k f^j(z) + R_0^{kj}$.

It can be seen that the above displacement field contains three primary variables (u_0, w_0, ψ_1) excluding the contribution from the potential variables ϕ^j. The number of the primary variables is thus the same as in the FSDT theory. Some unique features of the model developed are

(1) It incorporates the kinematic interactions between adjacent plies with different constitutive properties in presence of electromechanical field, even as the number of primary variables is independent of the number of layers and is the same as that of smeared first order theory.

(2) It accounts for the transverse normal strain induced by the electric field and hence can model non-uniform transverse displacement across the piezoelectric layers.

(3) The layerwise approximation of the electric potential enables effective modelling of the heterogeneity in the electric field across the thickness, induced by embedded or surface bonded piezoelectric sensor and actuator layers. The number of points N to be considered across the thickness for approximating the potential field can be chosen independent of the number of laminae L. The detail of approximation of the electric field can be selected based on the desired level of accuracy. The formulation allows for complete

neglect of the electric potential in the elastic layers since their dielectric constants are usually of much lower magnitude than those of the piezoelectric layers.

2.4. The governing equations

The equilibrium equations and the variationally consistent boundary conditions can be formulated in a weak form using the principle of virtual work given by:

$$\int_V (\sigma_i\,\delta\varepsilon_i + D_i\,\delta\phi_{,i})\,\mathrm{d}V = \int_A (p_i\,\delta u_i - q\,\delta\phi)\,\mathrm{d}A, \tag{16}$$

where V and A represent the volume and the surface of the piezoelectric continuum. $\int_V \sigma_i\,\delta\varepsilon_i\,\mathrm{d}V$ and $\int_V D_i\,\delta\phi_{,i}\,\mathrm{d}V$ represent the virtual work done respectively by the internal forces and the electric field. $\int_A p_i\,\delta u_i\,\mathrm{d}A$ and $\int_A q\,\delta\phi\,\mathrm{d}A$ are the virtual external works done by the applied surface tractions p_i and charge density q respectively. σ_i, ε_i, u_i and D_i denote respectively the components of stress, strain, displacement and electric displacement.

Making use in Eq. (16) of the kinematical Eqs. (5b) and (15) and the field-gradient Eq. (6), integrating it through the thickness and applying the Green's function to transfer all differentiations from the virtual displacements and potential to their coefficients, the integrals in Eq. (16) can be expressed as:

$$\begin{aligned}\int_V \sigma_i\,\delta\varepsilon_i\,\mathrm{d}V &= \int_V (\sigma_x\,\delta\varepsilon_x + \tau_{zx}\,\delta\gamma_{zx})\,\mathrm{d}V\\ &= \int_x \left[- N_{x,x}\,\delta u_0 - M_{x,xx}\,\delta w_0 - (P_{x,x} - Q_x)\,\delta\psi_1 + \sum_{j=1}^{N} (S^j_{x,xx} + \bar{Q}^j_{x,x})\,\delta\phi^j \right] \mathrm{d}x\\ &\quad + \Bigg[N_x\,\delta u_0 - (M_x\,\delta w_{0,x} - M_{x,x}\,\delta w_0) + P_x\,\delta\psi_1\\ &\qquad + \sum_{j=1}^{N} \{S^j_x\,\delta\phi^j_{,x} - (S^j_{x,x} + \bar{Q}^j_x)\,\delta\phi^j\} \Bigg]_x,\end{aligned} \tag{17}$$

$$\int_V D_i\,\delta\phi_{,i}\,\mathrm{d}V = \int_V (D_x\,\delta\phi_{,x} + D_z\,\delta\phi_{,z})\,\mathrm{d}z = -\int_x \sum_{j=1}^{N} (H^j_{,x} - G^j)\,\delta\phi^j \mathrm{d}x + \sum_{j=1}^{N} [H^j\,\delta\phi^j]_x, \tag{18}$$

where N_x, M_x, P_x, Q_x, S^j_x, $\bar{Q}^j_x$ are stress resultants and H^j, G^j are electric displacement resultants defined as

$$\begin{aligned} N_x &= \int_{-h/2}^{h/2} b\sigma_x\,\mathrm{d}z, \quad M_x = \int_{-h/2}^{h/2} bz\sigma_x\,\mathrm{d}z, \quad P_x = \sum_{k=1}^{L} \int_{z_{k-1}}^{z_k} bR_k(z)\sigma_x\,\mathrm{d}z,\\ Q_x &= \sum_{k=1}^{L} \int_{z_{k-1}}^{z_k} bR_k(z)_{,z}\tau_{zx}\,\mathrm{d}z, \quad S^j_x = \sum_{k=1}^{L} \int_{z_{k-1}}^{z_k} bF^j_k(z)\sigma_x\,\mathrm{d}z, \quad \bar{Q}^j_x = \sum_{k=1}^{L} b(\bar{e}^k_{15}/\bar{Q}^k_{55}) \int_{z_{k-1}}^{z_k} \Psi^j(z)\tau_{zx}\,\mathrm{d}z,\\ H^j &= \int_{-h/2}^{h/2} b\Psi^j(z)D_x\,\mathrm{d}z, \quad G^j = \int_{-h/2}^{h/2} b\Psi^j(z)_{,z}D_z\,\mathrm{d}z. \end{aligned} \tag{19}$$

Making use of Eq. (5b), the external work term in Eq. (16) can be expressed as:

$$\int_A (p_i\,\delta u_i - q\,\delta\phi)\,\mathrm{d}A = \int_x b[(p^1_z - p^2_z)\,\delta w_0 - (\bar{d}^1_{33}p^1_z\,\delta\phi^1 - \bar{d}^L_{33}p^2_z\,\delta\phi^N) - q^j\,\delta\phi^j]\,\mathrm{d}x, \tag{20}$$

where p_z^1 and p_z^2 are the normal pressures on the bottom and top surfaces of the beam and q^j are the surface charge densities at locations z^j.

Since the variations of the field variables can be arbitrary, their coefficients in Eq. (16) must be zero. Substituting expressions from Eqs. (17), (18) and (20) into Eq. (16), collecting the coefficients of (δu_0, δw_0, $\delta\psi_1$, $\delta\phi^j$) and setting them to zero, we obtain the equilibrium equations and the variationally consistent boundary conditions. The equilibrium equations thus obtained are:

$$\begin{aligned}
&\delta u_0 : N_{x,x} = 0,\\
&\delta w_0 : M_{x,xx} + f_z = 0,\\
&\delta\psi_1 : P_{x,x} - Q_x = 0,\\
&\delta\phi^j : H^j_{,x} - G^j - S^j_{x,xx} - \bar{Q}^j_{x,x} - b(q^j + \Gamma^j \bar{d}^j_{33} p^j_z) = 0, \quad (j = 1, 2, \ldots, N),
\end{aligned} \tag{21}$$

where $f_z = b(p_z^1 - p_z^2)$, $\Gamma^j = 1$ for $j = 1$ and $N = 0$; otherwise, $p_z^N = -p_z^2$ and $\bar{d}^N_{33} = \bar{d}^L_{33}$. The above equations are subject to the following essential or natural boundary conditions:

$$u_0 \text{ or } N_x; \quad w_0 \text{ or } M_{x,x}; \quad w_{0,x} \text{ or } M_x; \quad \psi_1 \text{ or } P_x; \quad \phi^j \text{ or } S^j_{x,x} + \bar{Q}^j_x - H^j; \quad \phi^j_{,x} \text{ or } S^j_x. \tag{22}$$

Relations between the resultants and the field variables are obtained by using Eqs. (4), (5b), (6) and (15) in Eq. (19), as follows:

$$\begin{aligned}
N_x &= A_{11}u_{0,x} - B_{11}w_{0,xx} + F_{11}\psi_{1,x} + \sum_{l=1}^{N}(\bar{F}^l_{11}\phi^l_{,xx} + \beta^l_1\phi^l),\\
M_x &= B_{11}u_{0,x} - D_{11}w_{0,xx} + E_{11}\psi_{1,x} + \sum_{l=1}^{N}(\bar{E}^l_{11}\phi^l_{,xx} + \beta^l_2\phi^l),\\
P_x &= F_{11}u_{0,x} - E_{11}w_{0,xx} + G_{11}\psi_{1,x} + \sum_{l=1}^{N}(\bar{G}^l_{11}\phi^l_{,xx} + \beta^l_3\phi^l),\\
S^j_x &= \bar{F}^j_{11}u_{0,x} - \bar{E}^j_{11}w_{0,xx} + \bar{G}^j_{11}\psi_{1,x} + \sum_{l=1}^{N}(\bar{H}^{jl}_{11}\phi^l_{,xx} + \beta^{jl}_4\phi^l),\\
Q_x &= D_{55}\psi_1, \quad \bar{Q}^j_x = \bar{D}^j_{55}\psi_1, \quad H^j = \bar{D}^j_{55}\psi_1 - \sum_{l=1}^{N}\hat{E}^{jl}_{11}\phi^l_{,x},\\
G^j &= \beta^j_1 u_{0,x} - \beta^j_2 w_{0,xx} + \beta^j_3\psi_{1,x} + \sum_{l=1}^{N}(\beta^{lj}_4\phi^l_{,xx} + \beta^{jl}_5\phi^l);
\end{aligned} \tag{23}$$

with

$$\begin{aligned}
&[A_{11}, B_{11}, D_{11}, F_{11}, E_{11}, G_{11}] = \int_{-h/2}^{h/2} b\bar{Q}_{11}[1, z, z^2, R_k(z), zR_k(z), R_k^2(z)]\,\mathrm{d}z,\\
&[F^j_{11}, E^j_{11}, G^j_{11}, H^{jl}_{11}] = \int_{-h/2}^{h/2} b\bar{Q}_{11}F^j_k(z)[1, z, R_k(z), F^l_k(z)]\,\mathrm{d}z,\\
&[\beta^l_1, \beta^l_2, \beta^l_3, \beta^{jl}_4] = \int_{-h/2}^{h/2} b\bar{e}_{31}[1, z, R_k(z), F^j_k(z)]\Psi^l(z)_{,z}\,\mathrm{d}z, \quad \bar{\beta}^{jl}_5 = \int_{-h/2}^{h/2} b\bar{\eta}_{33}\Psi^j_{,z}\Psi^l_{,z}\,\mathrm{d}z,\\
&D_{55} = \int_{-h/2}^{h/2} b\bar{Q}_{55}(R_{k,z})^2\,\mathrm{d}z, \quad \bar{D}^j_{55} = \int_{-h/2}^{h/2} b\bar{e}_{15}\Psi^j(z)R_{k,z}\,\mathrm{d}z.
\end{aligned} \tag{24}$$

Substitution of the expressions from Eq. (23) into Eqs. (21) yields the following electromechanical equilibrium equations in terms of the primary field variables $(u_0, w_0, \psi_1, \phi^j)$:

$$[L_{ij}]\bar{U} = P, \tag{25}$$

where $\bar{U} = [u_0\, w_0\, \psi_1\, \phi^1\, \phi^2 \ldots \phi^N]^{\mathrm{T}}$, $P = [0\, f_z\, 0\, \bar{q}^1\, \bar{q}^2 \ldots \bar{q}^N]^{\mathrm{T}}$ with $\bar{q}^l = b(q^l - \Gamma^l \bar{d}^l_{33} p^l_z)$. L_{ij} are linear differential operators with $L_{ij} = L_{ji}$ given by

$$\begin{aligned}
&L_{11} = A_{11}(\ )_{,xx}, \quad L_{12} = -B_{11}(\ )_{,xxx}, \quad L_{13} = F_{11}(\ )_{,xx}, \quad L_{1,3+l} = \bar{F}^l_{11}(\ )_{,xxx} + \beta^l_1(\ )_{,x},\\
&L_{22} = D_{11}(\ )_{,xxxx}, \quad L_{23} = -E_{11}(\ )_{,xxx}, \quad L_{2,3+l} = -\bar{E}^l_{11}(\ )_{,xxxx} - \beta^l_2(\ )_{,xx}, \quad L_{33} = G_{11}(\ )_{,xx} - D_{55},\\
&L_{3,3+l} = \bar{G}^l_{11}(\ )_{,xxx} + \beta^l_3(\ )_{,x}, \quad L_{3+m,3+l} = \bar{H}^{ml}_{11}(\ )_{,xxxx} + (\beta^{ml}_4 + \beta^{lm}_4)(\ )_{,xx} + \hat{E}^{ml}_{11}(\ )_{,xx} - \beta^{ml}_5, (m,l) = 1, \ldots, N.
\end{aligned} \tag{26}$$

The above system of ordinary differential equations is solved for given electromechanical loads and boundary conditions. The transverse shear stress τ_{zx} can be obtained in two ways: (i) directly from the constitutive equations as given in Eq. (7) and (ii) by integrating the 3D stress equilibrium equation as $\tau_{zx} = -\int_{-h/2}^{z} \sigma_{x,x}\, \mathrm{d}z$.

3. Analytical solution for a simply supported hybrid beam

In order to demonstrate the accuracy, applicability and robustness of the coupled piezoelectric laminate theory developed above, an analytical solution is obtained for a hybrid beam of span a with simply supported ends. With reference to Eq. (22), the boundary conditions at the simply supported ends are

$$N_x = w_0 = M_x = P_x = \phi_j = S^j_x = 0, \quad j = 1, \ldots, N \quad \text{at } x = 0, a. \tag{27}$$

The solution of Eq. (25), which identically satisfies the boundary conditions given by Eq. (27), is expressed in terms of Fourier Series as:

$$\begin{aligned}
(w_0, \phi^j, N_x, M_x, P_x, S^j_x, G^j) &= \sum_{n=1}^{\infty} (w_0, \phi^j, N_x, M_x, P_x, S^j_x, G^j)_n \sin \bar{n}x,\\
(u_0, \psi_1, Q_x, \bar{Q}^j_x, H^j) &= \sum_{n=1}^{\infty} (u_0, \psi_1, Q_x, \bar{Q}^j_x, H^j)_n \cos \bar{n}x
\end{aligned} \tag{28}$$

with $\bar{n} = n\pi/a$. The applied load f_z and the applied charge density q^j are also similarly expanded in Fourier series as

$$(f_z, q^j) = \sum_{n=1}^{\infty} (f_z, q^j)_n \sin \bar{n}x. \tag{29}$$

Substituting the expressions from Eqs. (28) and (29) into the equilibrium Eqs. (25) yields the following coupled system of linear algebraic equations for the nth Fourier component.

$$\begin{bmatrix} X^{uu} & X^{ue} \\ X^{eu} & X^{ee} \end{bmatrix} \begin{Bmatrix} U^n \\ \Phi^n \end{Bmatrix} = \begin{Bmatrix} F^n \\ Q^n \end{Bmatrix} \tag{30}$$

The submatrices X^{uu}, X^{ue}, X^{eu}, X^{ee} are of sizes 3×3, $3\times N$, $N\times 3$ and $N\times N$ respectively and are given by

$$\begin{aligned}
&X^{uu}_{11}=\bar{n}^2A_{11},\quad X^{uu}_{12}=-\bar{n}^3B_{11},\quad X^{uu}_{13}=\bar{n}^2F_{11},\quad X^{uu}_{22}=\bar{n}^4D_{11},\quad X^{uu}_{23}=-\bar{n}^3E_{11},\quad X^{uu}_{33}=\bar{n}^2G_{11}+D_{55},\\
&X^{uu}_{ji}=X^{uu}_{ij};\quad X^{ue}_{1l}=\bar{n}^3\bar{F}^l_{11}-\bar{n}\beta^l_1,\quad X^{ue}_{2l}=-(\bar{n}^4\bar{E}^l_{11}-\bar{n}^2\beta^l_2),\quad X^{ue}_{3l}=\bar{n}^3\bar{G}^l_{11}-\bar{n}\beta^l_3;\quad X^{eu}_{li}=X^{ue}_{il};\\
&X^{ee}_{ml}=-[\bar{n}^4\bar{H}^{ml}_{11}+\bar{n}^2(\beta^{ml}_4+\beta^{lm}_4)+\hat{E}^{ml}_{11}\bar{n}^2+\beta^{ml}_5],\quad X^{ee}_{lm}=X^{ee}_{ml},\quad (i,j)=1,2,3,\ (l,m)=1,\ldots,N;\\
&F^n=[0\ f_z\ 0]^{\mathrm{T}},\quad Q^n=[\bar{q}^1\ \bar{q}^2\ldots\bar{q}^N]^{\mathrm{T}}_n,\quad U^n=[u_0\ w_0\ \psi_1]^{\mathrm{T}}_n,\quad \Phi^n=[\bar{\phi}^1\ \bar{\phi}^2\ldots\bar{\phi}^N]^{\mathrm{T}}_n.
\end{aligned}\tag{31}$$

Considering that both sensory and active piezoelectric layers can be present in the laminate, the electric potential vector Φ is subdivided into an unknown sensory component Φ_s representing the voltage output at the sensors and a known active component Φ_a representing the applied voltage at the actuators such that $\Phi=[\Phi_s;\Phi_a]$. In accordance with the selected sensing and actuation configuration, Eq. (30) can be partitioned and arranged in the following form:

$$\begin{bmatrix} X^{uu} & X^{ue}_{ss}\\ X^{eu}_{ss} & X^{ee}_{ss}\end{bmatrix}\begin{Bmatrix} U^n\\ \Phi^n_s\end{Bmatrix}=\begin{Bmatrix} F^n-X^{ue}_{sa}\Phi^n_a\\ Q^n_s-X^{ee}_{sa}\Phi^n_a\end{Bmatrix}\tag{32}$$

It may be mentioned here that it is possible in the above coupled form of equations to model the response of the piezoelectric beam structure either in active or sensory or combined active-sensory mode.

4. Numerical results and discussion

The numerical illustrations presented in this section concern the assessment of the coupled zigzag displacement – layerwise potential model in regard to its accuracy, its ability to capture the electromechanical coupling phenomena and its robustness in modelling practical hybrid beam configurations in sensory, active or combined mode. In order to validate the computer program developed for the numerical illustrations, results are obtained for a simply supported elastic composite flat panel in cylindrical bending subjected to a single term mechanical loading $f_z=p_0\sin(\bar{n}x)$, for which the present solution is modified by using appropriate constitutive equations. The panel is made up of an asymmetric $[0°/90°/0°/90°]$ laminate with the following properties of the $0°$ layer: $(Y_1,Y_2,G_{12},G_{23})=(25,1,0.5,0.2)\times 10^6$ psi, $G_{13}=G_{12}$, $\nu_{12}=\nu_{13}=\nu_{23}=0.25$, $d_{ij}=0$. Here Y_i, G_{ij} and ν_{ij} are the Young's moduli, shear moduli and Poisson's ratios respectively. The results obtained for span-to-thickness ratios $S=a/h=4$, 6 are compared in Table 1 with the elastic third order zigzag theory results presented by Cho and Parmerter (1993) wherein the response entities are non-dimensionalised as $\hat{w}=100Y_1w/hS^4p_0$, $\hat{u}=Y_1u/hp_0$, $\hat{\sigma}_x=\sigma_x/p_0$, $\hat{\tau}_{zx}=\tau_{zx}/p_0$. The results for

Table 1
Response of an elastic multilayered beam under sinusoidal pressure load

	$S=a/h$	Present	Cho and Parmerter (1993)
$\hat{w}(0.5a,0)$	4	4.083	4.083
	6	2.501	2.501
$\hat{u}(0,0.5h)$	4	−1.355	−1.35[a]
	6	−3.698	−3.70[a]
$\hat{\sigma}_x(0.5a,0.5h)$	4	26.68	26.7[a]
	6	48.52	48.5[a]
$\hat{\tau}_{zx}(0,0)$	4	1.952	1.95[a]
	6	3.064	3.06[a]

[a] Read from graphical representation.

$\hat{u}$, $\hat{\sigma}_x$ and $\hat{\tau}_{zx}$ have been read from their graphical representations in the above reference. The two results are found to be in excellent agreement.

Detailed results are presented for simply supported hybrid beams made up of a substrate of graphite-epoxy composite with piezoelectric layer(s) of PZT-5A bonded to its surface(s). All plies of the substrate have equal thickness. The ratio of the piezoelectric layer thickness h_p to the laminate thickness h has been taken as 0.1 unless mentioned otherwise. The properties of graphite-epoxy composite are selected as (Xu et al., 1995):

$$(Y_L, Y_T, G_{LT}, G_{TT}) = (181, 10.3, 7.17, 2.87)\ \text{GPa}, \quad d_{ij} = 0, \quad (v_{LT}, v_{TT}) = (0.28, 0.33),$$
$$(\eta_{LL}, \eta_{TT}) = (30.96, 26.53) \times 10^{-12}\text{F/m},$$

where L and T denote directions parallel and transverse to the fibres. The properties of PZT are taken as (Xu et al., 1995):

$$(Y_1, Y_2, Y_3, G_{12}, G_{23}, G_{31}) = (61.0, 61.0, 53.2, 22.6, 21.1, 21.1)\ \text{GPa},$$
$$(v_{12}, v_{13}, v_{23}) = (0.35, 0.38, 0.38),$$
$$(d_{31}, d_{32}, d_{33}, d_{15}, d_{24}) = (-171, -171, 374, 584, 584) \times 10^{-12}\text{m/V},$$
$$(\eta_{11}, \eta_{22}, \eta_{33}) = (1.53, 1.53, 1.50) \times 10^{-8}\,\text{F/m}.$$

The following lamination schemes are considered with the orientation of the fibres given relative to x-axis and stacking order mentioned from top to bottom:

(a) Symmetric substrate laminate with PZT layer bonded to its top face [p/0°/90°/90°/0°]. The letter p indicates the piezoelectric layer.
(b) Asymmetric substrate laminate with PZT layer bonded to its top face [p/0°/90°/0°/90°].
(c) Symmetric eight-layered substrate with PZT layer bonded to both top and bottom faces $[\text{p}/0°/90°/\pm 45°]_s$.

The first two laminates have been selected to assess the results of hybrid beams with symmetric and asymmetric crossply laminates for the substrate against the available exact solutions. The laminate type c has been chosen to present results for hybrid beams with a more general laminate configuration for the substrate consisting of angle-ply laminae.

Following mechanical and electrical loads are considered:

1. A sinusoidal pressure on the top surface, $p_z^2 = p_0 \sin(\pi x/a)$;
2. An actuating potential applied at the top surface, $\phi^N = \phi_0 \sin(\pi x/a)$.

The interface of each PZT layer with the substrate is grounded (zero potential) for all applications. The results for these loads are non-dimensionalised as follows with $S = a/h$, $d_T = 374 \times 10^{-12}$ CN^{-1}:

1. $(\bar{u}, \bar{w}) = 100(u, w/S)Y_T/hS^3p_0$, $(\bar{\sigma}_x, \bar{\tau}_{zx}) = (\sigma_x/S, \tau_{zx})/Sp_0$, $\bar{\phi} = 10^4\phi Y_T d_T/hS^2p_0$, $\bar{D}_z = D_z/d_T p_0$;
2. $(\tilde{u}, \tilde{w}) = 10(u, w/S)/Sd_T\phi_0$, $(\tilde{\sigma}_x, \tilde{\tau}_{zx}) = (\sigma_x/10, S\tau_{zx})h/Y_T d_T\phi_0$, $\tilde{\phi} = \phi/\phi_0$, $\tilde{D}_z = D_z h/100Y_T d_T^2\phi_0$.

4.1. Beam with sensory piezoelectric layer under mechanical load

The accuracy of the developed coupled model in predicting response of a sensory hybrid beam subjected to the mechanical load of case 1 is investigated by comparing the results for beams of types a and b with symmetric and asymmetric substrate laminates with an exact piezoelectric solution. The exact 3D solution

for hybrid composite plates in cylindrical bending (Brooks and Heyliger, 1994; Kapuria et al., 1997a) has been modified slightly to make it applicable for beams by using appropriate constitutive equations. The exact solution considers $\sigma_y = 0$, $\tau_{yz} = 0$, $\tau_{xy} = 0$ but $\sigma_z \neq 0$. The edge boundary conditions are taken as $w = 0$, $\sigma_x = 0$ and $\phi = 0$ at $x = 0$, a. No a priori assumptions are made on the through-the-thickness distributions of the response entities. These are obtained by exactly solving the governing field equations of coupled piezoelasticity subject to the exact satisfaction of the boundary and interface continuity conditions. FSDT results with shear correction factor $k_{55}^2 = 5/6$ are also presented for comparison. Shear $\bar{\tau}_{zx}$ in FSDT is obtained by integrating the equilibrium equation. The top surface of the sensory layer is kept at charge free condition (i.e. open-circuit condition). For the purpose of discretising the electric field across the thickness, the piezoelectric layer is divided into four layers.

The results for the mid-surface deflection $\bar{w}$, inplane displacement $\bar{u}$, normal stress $\bar{\sigma}_x$ in the substrate and the piezoelectric layer, transverse shear stress $\bar{\tau}_{zx}$ predicted from the constitutive equation and the equilibrium equation and the induced potential $\bar{\phi}$ at the sensory layer are compared in Table 2 for three values of S viz. 4 (thick beam), 10 (moderately thick beam) and 100 (thin beam). The through-the-thickness distributions of $\bar{u}$, $\bar{w}$, $\bar{\sigma}_x$ and $\bar{\tau}_{zx}$ for thick and moderately thick beams of types a and b are shown in Figs. 2–4. The distribution of the induced sensory potential across the piezoelectric layer is shown in Fig. 5. It is observed that the present results for $\bar{u}$, $\bar{w}$ and $\bar{\sigma}_x$ are in good agreement with the exact solution for both thick and thin hybrid beams with symmetric and asymmetric substrate laminates. The non-linear through-the-thickness distributions of $\bar{u}$ and $\bar{\sigma}_z$ with slope discontinuities at interfaces have been very well captured by the present theory. In contrast, FSDT has yielded far inferior results even for a moderately thick beam with $S = 10$. While FSDT underestimates the central deflection $\bar{w}$ and the inplane displacement $\bar{u}$ at top face respectively by 12.4% and 8.1% for a moderately thick beam of type a, the corresponding errors in the

Table 2
Comparison of results for sensory beams under pressure load of case 1

	S	Beam a [p/0°/90°/90°/0°] ($h_p/h = 0.1$)			Beam b [p/0°/90°/0°/90°] ($h_p/h = 0.1$)		
		Exact	FSDT/exact	Present/exact	Exact	FSDT/exact	Present/exact
$\bar{w}$(0.5a,0)	4	−3.0636	0.688	0.997	−4.0352	0.734	0.997
	10	−1.2971	0.875	0.996	−2.1656	0.919	0.995
	100	−0.9444	1.008	1.000	−1.7873	1.011	1.000
$\bar{u}$(0,0.5h)	4	2.4785	0.623	0.958	3.2611	0.736	0.970
	10	1.6797	0.919	0.989	2.5113	0.956	0.993
	100	1.5218	1.014	1.000	2.3610	1.016	1.000
$\bar{\sigma}_x$(0.5a,0.5h)	4	−0.5140	0.559	0.905	−0.6718	0.665	0.929
	10	−0.3409	0.842	0.975	−0.5086	0.878	0.982
	100	−0.3068	0.936	0.998	−0.4760	0.938	0.998
$\bar{\sigma}_x(0.5a, 0.4^- h)$	4	−0.8478	0.810	0.953	−1.1177	0.905	0.969
	10	−0.7065	0.972	0.988	−1.0157	0.996	0.993
	100	−0.6764	1.016	1.000	−0.9935	1.018	1.000
$\bar{\tau}_{zx}(0,0)$	4	−0.4063	1.086	1.005 (1.033)	−0.5373	1.100	1.013 (0.938)
	10	−0.4343	1.016	1.002 (1.003)	−0.5794	1.020	1.003 (0.907)
	100	−0.4402	1.003	1.000 (0.997)	−0.5886	1.004	1.000 (0.892)
$\bar{\phi}(0.5a, 0.5h)$	4	7.896	–	0.852	11.530	–	0.903
	10	7.920	–	0.974	11.914	–	0.983
	100	7.884	–	1.000	11.944	–	1.000

The values for $\bar{\tau}_{zx}$ given within brackets ( ) are obtained directly from the constitutive equation.

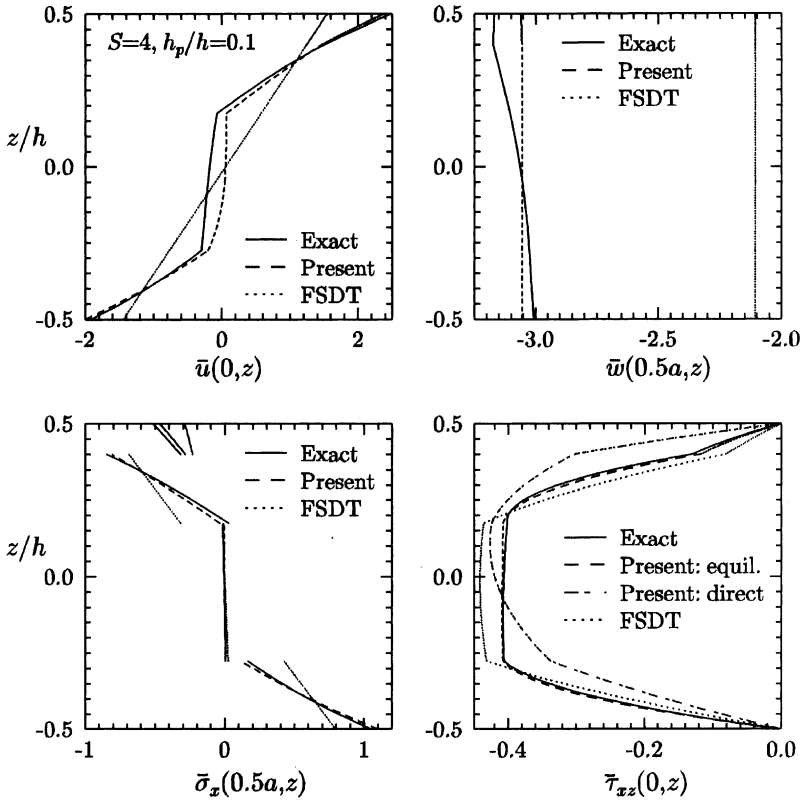

Fig. 2. Through-the-thickness distributions of $\bar{u}$, $\bar{w}$, $\bar{\sigma}_x$, $\bar{\tau}_{zx}$ for thick ($S = 4$) sensory beam a under pressure load.

present results are only 0.4% and 1% respectively. Similarly, the error in predicted inplane stress $\bar{\sigma}_x$ in the sensor layer reduces from as high as 15.8% in case of FSDT to 2.5% in the present case for the above beam. The improvement in the present results over FSDT become more pronounced for thicker beams, wherein simplified kinematic assumptions do not hold well. The shear stress distribution obtained by integrating equilibrium equation using the present theory is also in excellent agreement with the exact solution for both thin and thick beams. The direct constitutive approach yields comparatively less accurate shear distribution, but predicts the maximum shear stress quite accurately. Of particular importance is the ability of the present theory to predict sensory potential with very good accuracy for thin to moderately thick beams. It can be seen from Table 2 and Fig. 5 that the error in the predicted sensory potential is only 2.6% and 1.7% for intermediate thick beams of types a and b respectively. The deviation almost vanishes (<0.03%) for thin beams with $S = 100$.

The top surface of the sensor layer can be subjected to two electric conditions: (1) open-circuit condition wherein the applied charge density on the surface is zero as stated before and (2) closed-circuit condition wherein the surface is kept at an imposed potential (equal to zero). Results for the transverse displacement and the electric potential of a thick sensory beam of type a with the above two electric conditions are presented in Fig. 6 for two values of the sensory layer thickness ratio $h_p/h = 0.1$ and 0.2. It is observed that the electric boundary conditions have a definite effect on the value as well as the across-the-thickness distribution of $\bar{w}$ as a result of different electric fields induced in the piezoelectric layer by piezoelectric coupling. The effect becomes more pronounced for higher thickness of the piezoelectric layer. It reveals that

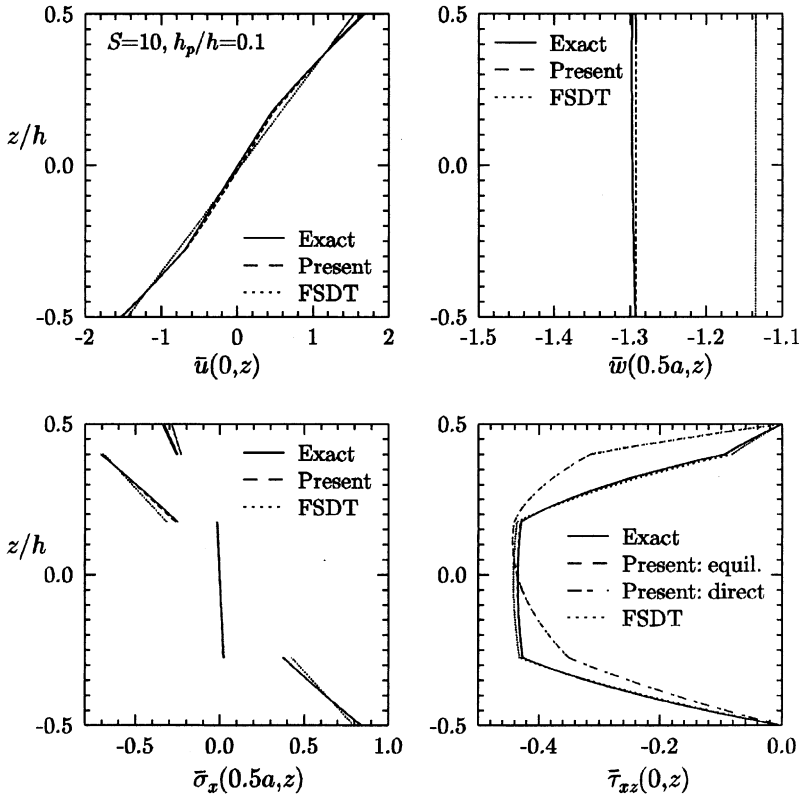

Fig. 3. Through-the-thickness distributions of $\bar{u}$, $\bar{w}$, $\bar{\sigma}_x$, $\bar{\tau}_{zx}$ for moderately thick ($S = 10$) sensory beam a under pressure load.

the piezoelectric coupling effect increases with the increase in the piezolayer thickness to overall thickness ratio. The slight variation in $\bar{w}$ in the piezoelectric layer as a result of the transverse strain induced due to non-zero d_{33} piezoelectric constant has been very well captured by the present theory.

4.2. Beam with piezoelectric actuator layer under actuation potential

In this case, beams a and b are analysed for an actuation potential of case 2 imposed on the top surface of the piezoelectric layer. The predicted results for $\tilde{w}$ at the middle and top surfaces, $\tilde{u}$ at the top surface, $\tilde{\sigma}_x$ at the substrate and the actuator layer, $\tilde{\tau}_{zx}$ at the actuator-substrate interface obtained by the direct approach (from the constitutive equation) and the post-processing approach (from the equilibrium equation) and $\tilde{D}_z$ at the top surface of the actuator are presented in Table 3 for $S = 4$, 10 and 100. The corresponding results of exact solution and FSDT solution are also tabulated for comparison. The through-the-thickness variations of $\tilde{u}$, $\tilde{w}$, $\tilde{\sigma}_x$ and $\tilde{\tau}_{zx}$ are shown in Figs. 7–9. The results depict that the present theory has captured the through-the-thickness variation of $\tilde{w}$ quite well even for a thick laminate as a result of the inclusion of the out-of-plane normal strain induced by the electric field through the piezoelectric constant d_{33}. The improvement of the present theory over FSDT in predicting $\tilde{w}$ is very significant. The error in mid-surface deflection reduced from 42.2% in FSDT to 5.6% in the present theory for a thick beam a with $S = 4$. For an intermediate thick beam a ($S = 10$), the deviations of the FSDT and the present results for the same from

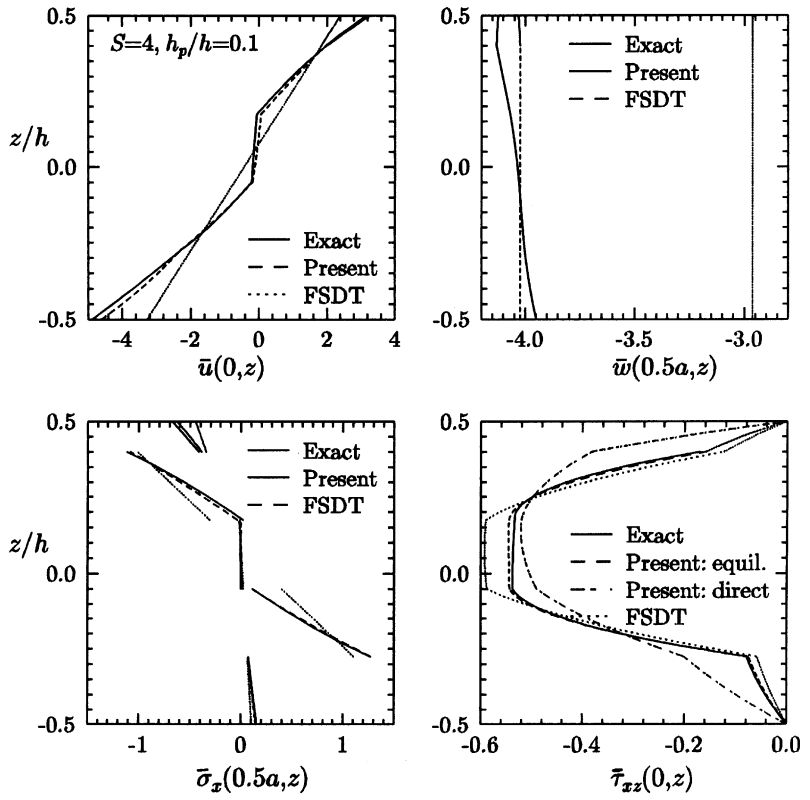

Fig. 4. Through-the-thickness distributions of $\bar{u}$, $\bar{w}$, $\bar{\sigma}_x$, $\bar{\tau}_{zx}$ for thick ($S = 4$) sensory beam b under pressure load.

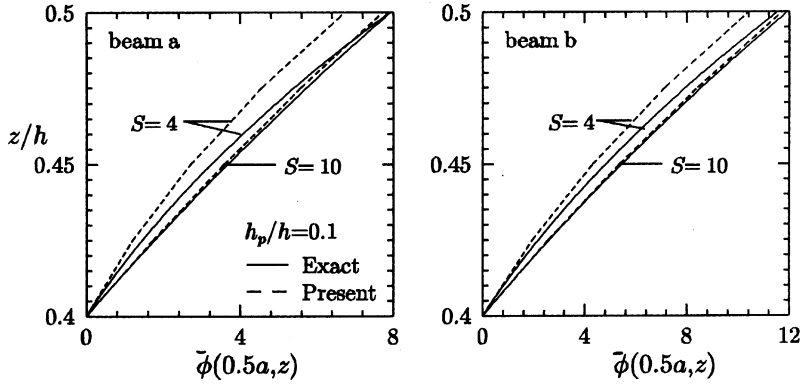

Fig. 5. Distribution of sensory potential across the sensor layer of beams a and b under pressure load.

the exact solution are 9.9% and 1.8% respectively. The present theory shows improvement over FSDT in predicting $\tilde{u}$ and $\tilde{\sigma}_x$ too. It, however, yields very poor estimate of $\tilde{\tau}_{zx}$, when computed directly from the

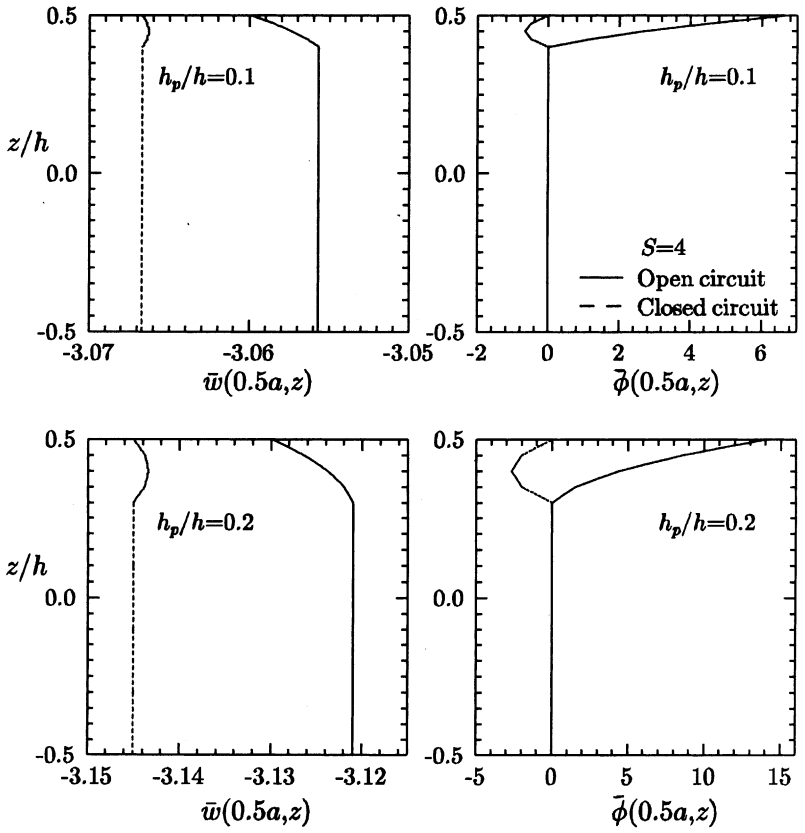

Fig. 6. Effect of electric boundary conditions on $\bar{w}$ and $\bar{\phi}$ of a thick sensory beam a under pressure load with sensor layer thickness ratio $h_p/h = 0.1, 0.2$.

constitutive equation. The reason for the same can be traced to the absence of a layerwise linear term in the expression of $\tilde{\tau}_{zx}$ in Eq. (7). $\tilde{\tau}_{zx}$ computed from the equilibrium equation, of course, yielded excellent agreement with the exact solutions for all thickness ratios and laminate configurations. The predicted results for the accumulated electric displacement $\tilde{D}_z$ at the top surface of the actuated piezoelectric layer match closely with the exact solution.

4.3. Combined sensing and actuation for deflection control

This example considers a hybrid beam of type c consisting of a more general laminate configuration $[0°/90°/\pm 45°]_s$ for the substrate with a piezoelectric layer bonded to its either surface. The bottom piezoelectric layer acts as a sensor in open-circuit condition i.e. its bottom surface is kept charge-free. The upper piezoelectric layer is used to compensate the mechanical deflections by applying proper actuation potential to its top surface. The mid-surface deflections of the beam under a sinusoidal pressure load of case 1 and the actuation potential of case 2 with $\bar{\phi}_0 = 0$, 400, 800 are plotted in Fig. 10. It is seen that the deflection induced by the pressure load is reduced substantially with the application of an actuation potential of $\bar{\phi}_0 = 800$. The sensory potentials measured at the bottom surface of the sensor layer (ϕ^1) for different actuation voltages are also shown in Fig. 10.

Table 3
Comparison of results for actuated beams under potential load of case 2

	S	Beam a [p/0°/90°/90°/0°] ($h_p/h = 0.1$)			Beam b [p/0°/90°/0°/90°] ($h_p/h = 0.1$)		
		Exact	FSDT/exact	Present/exact	Exact	FSDT/exact	Present/exact
$\tilde{w}$(0.5a,0)	4	1.7370	0.577	0.944	2.2938	0.705	0.958
	10	1.2837	0.901	0.982	1.8887	0.938	0.988
	100	1.1866	0.999	1.000	1.8010	0.999	1.000
$\tilde{w}$(0.5a,0.5h)	4	1.1942	0.840	0.850	1.7465	0.926	0.901
	10	1.1923	0.970	0.974	1.7971	0.985	0.983
	100	1.1857	1.000	1.000	1.8000	1.000	1.000
$\tilde{u}$(0,0.5h)	4	−3.638	0.794	0.859	−4.022	0.834	0.883
	10	−3.017	0.957	0.970	−3.470	0.967	0.976
	100	−2.890	0.999	1.000	−3.557	0.943	0.943
$\tilde{\sigma}_x$(0.5a,0.5h)	4	−2.032	1.068	1.047	−1.959	1.063	1.045
	10	−2.144	1.012	1.008	−2.058	1.012	1.008
	100	−2.167	1.001	1.000	−2.079	1.002	1.000
$\tilde{\sigma}_x$(0.5a,0.4$^-$h)	4	1.617	0.859	0.875	1.734	0.889	0.896
	10	1.429	0.972	0.975	1.574	0.979	0.980
	100	1.389	1.000	1.000	1.541	1.000	1.000
$\tilde{\tau}_{zx}$(0,0.4h)	4	−6.583	1.052	1.041	−6.409	1.047	1.038
				(0.099)			(0.107)
	10	−6.868	1.009	1.007	−6.659	1.008	1.006
				(0.099)			(0.106)
	100	−6.927	1.000	1.000	−6.710	1.000	1.000
				(0.099)			(0.106)
$\tilde{D}_z$(0.5a,0.5h)	4	−1.512	–	0.997	−1.515	–	0.997
	10	−1.505	–	1.000	−1.508	–	1.000
	100	−1.504	–	1.000	−1.507	–	1.001

The values for $\tilde{\tau}_{zx}$ given within brackets ( ) are obtained directly from the constitutive equation.

5. Conclusions

A novel coupled electromechanical model has been presented for the static analysis of multilayered composite beams with surface bonded or embedded piezoelectric layers. The model combines a third order zigzag representation of the inplane displacement with a layerwise representation of the electric potential such that the interlaminar shear stress continuity conditions and shear free conditions on the top and bottom surfaces are satisfied a priori under general electromechanical loading condition. The model also includes the piezoelectric transverse normal strain which enables it to capture the non-uniform variation of the deflection across the piezoelectric layers. The number of primary variables for the mechanical field is the same as that of FSDT. Thus the model preserves the computational advantage of an ESL theory while allowing for important local through-the-thickness variations of displacements and stresses and maintaining sufficient detail in the approximation of electric fields.

The accuracy, applicability and robustness of the proposed theory have been demonstrated by obtaining an analytical solution for simply supported hybrid beams and comparing the results with the exact piezoelastic solution and the uncoupled FSDT solution. The results depict that, overall, the developed mechanics yields very good prediction of global as well as local laminate level response for both thin and thick smart composite beams with symmetric or asymmetric laminate for the substrate. For the mechanical load case, the present results for the deflection, the non-linear through-the-thickness variations of the inplane displacement, the inplane normal stress and the transverse shear stress and the open circuit potential developed in the sensor layer are in excellent agreement with exact solution for thin to intermediate thick beams. The

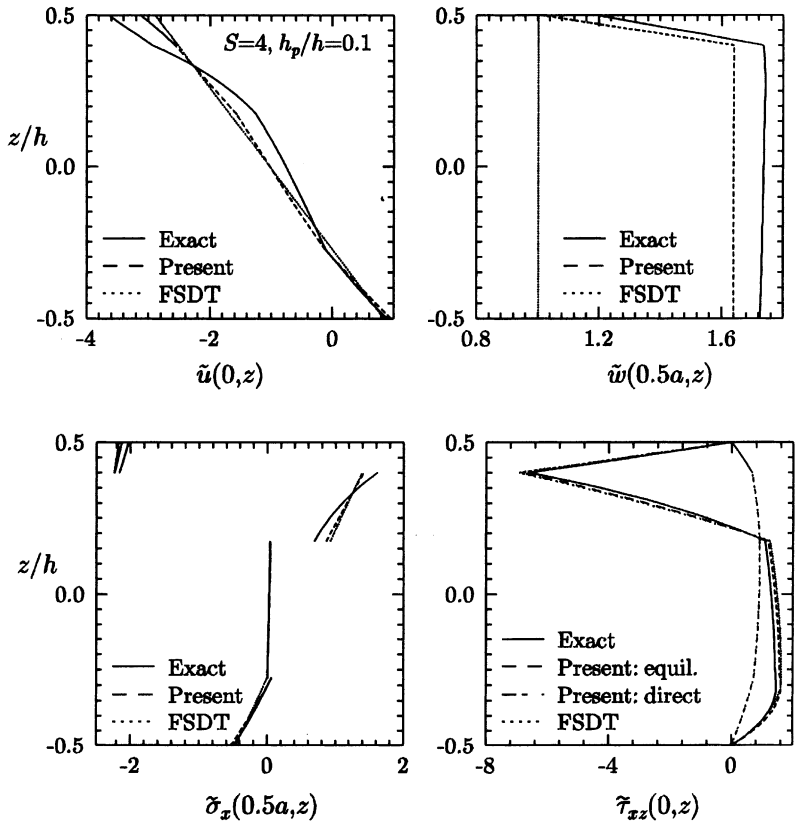

Fig. 7. Through-the-thickness distributions of $\tilde{u}$, $\tilde{w}$, $\tilde{\sigma}_x$, $\tilde{\tau}_{zx}$ for thick ($S = 4$) active beam a under electric potential load.

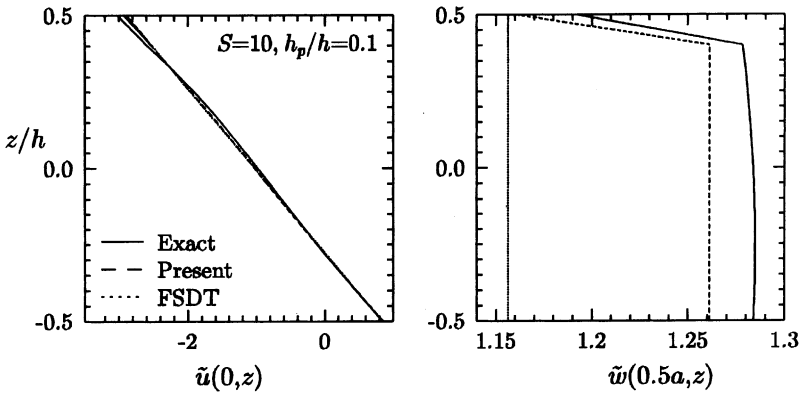

Fig. 8. Through-the-thickness distributions of $\tilde{u}$ and $\tilde{w}$ for moderately thick ($S = 10$) active beam a under electric potential load.

agreement is good in case of thicker beams too. The accuracy level increases drastically with the increase of span-to-thickness ratio. For the potential load case, the deflection including its variation across the actuator layer, the inplane displacement, the normal stress and the electric displacement developed at the actuated

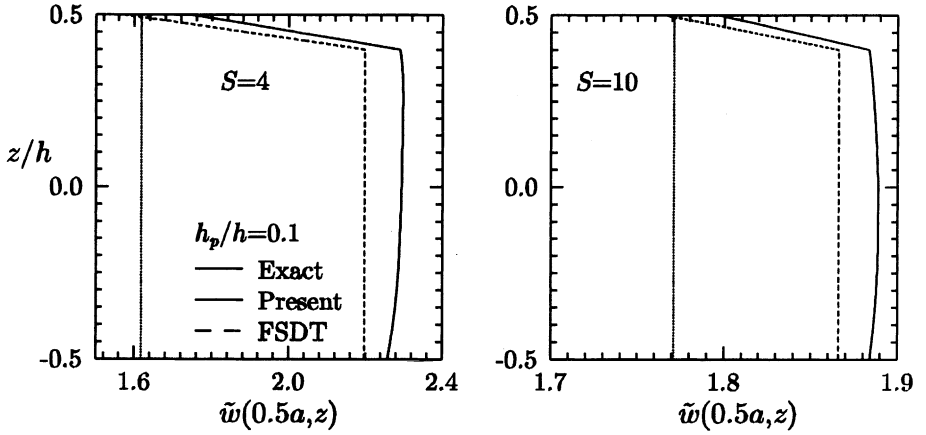

Fig. 9. Through-the-thickness distribution of $\tilde{w}$ for active beam b under electric potential load.

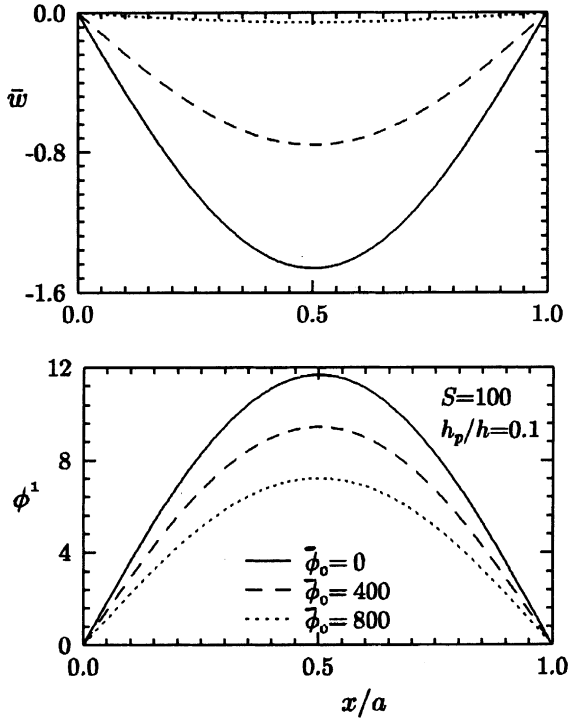

Fig. 10. Mid-surface deflection $\bar{w}$ and measured sensory potential $\bar{\phi}$ of a sensory/active beam c under pressure load with different actuation potentials $\bar{\phi}_0$.

surface compare very well with the 3D solution for all lamination schemes. The shear stress in this case is, however, very poorly predicted when computed directly from the constitutive equations. The error is due to the absence of a layerwise linear term in the expression of the transverse shear stress. The shear stress computed by integrating the equilibrium equation is again in close agreement with the exact solution.

Comparison of the present results with FSDT solution has established the superiority of the developed model over FSDT for all applications. The applications discussed here demonstrated the capability of the proposed formulation to model sensory, active and combined response of smart composite beams.

Work is in progress to extend the model to the dynamics and control of smart beams. Moreover, application of the formulation to general problems with different geometry and boundary conditions will require development of a numerical method of solution such as the finite element method. Work in this regard will be taken up in future.

Acknowledgements

The author is thankful to the reviewers for their constructive comments and useful suggestions which have improved the quality of the paper. The author is also grateful to Professor P.C. Dumir of IIT Delhi, India, for taking active interest and giving valuable suggestions through out this work.

References

Auld, B.A., 1973. Acoustic Fields and Waves in Solids, vol I. Wiley, New York, pp. 271–272.

Brooks, S., Heyliger, P., 1994. Static behavior of piezoelectric laminates with distributed and patched actuators. J. Int. Mat. Syst. Struct. 5, 635–646.

Cho, M., Parmerter, R.R., 1993. Efficient higher order composite plate theory for general lamination configurations. AIAA J. 31, 1299–1306.

Cho, M., Parmerter, R.R., 1994. Finite element for composite plate bending based on efficient higher order theory. AIAA J. 32, 2241–2248.

Crawley, E.F., Lazarus, K.B., 1991. Induced strain actuation of isotropic and anisotropic plates. AIAA J. 29, 944–951.

Ha, S.K., Keilers, C., Chang, F.K., 1992. Finite element analysis of composite structures containing distributed piezoceramic sensors and actuators. AIAA J. 30, 772–780.

Heyliger, P., 1994. Static behavior of laminated elastic/piezoelectric plates. AIAA J. 32, 2481–2484.

Heyliger, P.R., Ramirez, G., Saravanos, D.A., 1994. Coupled discrete-layer finite elements for laminated piezoelectric plates. Comm. Num. Meth. Engng. 10, 971–981.

Huang, J.H., Wu, T.L., 1996. Analysis of hybrid multilayered piezoelectric plates. Int. J. Engng. Sci. 34, 171–181.

Jonnalagadda, K.D., Blandford, G.E., Tauchert, T.R., 1994. Piezothermoelastic composite plate analysis using first-order shear deformation theory. Comput. Struct. 51, 79–89.

Kapuria, S., Dube, G.P., Dumir, P.C., 1997a. Exact piezothermoelastic solution for simply supported laminated flat panel in cylindrical bending. ZAMM 77, 281–293.

Kapuria, S., Dube, G.P., Dumir, P.C., Sengupta, S., 1997b. Levy-type piezothermoelastic solution for hybrid plate using first order shear deformation theory. Composites Part B: Engineering 28, 535–546.

Lee, C.K., Moon, F.C., 1989. Laminated piezopolymer plates for torsion and bending sensors and actuators. J. Acoust. Soc. Am. 85, 2432–2439.

Lee, C.K., 1990. Theory of laminated piezoelectric plates for the design of distributed sensors/actuators. Part 1: Governing equations and reciprocal relationships.. J. Acoust. Soc. Am. 87, 1144–1158.

Lee, J.S., Jiang, L.Z., 1996. Exact electroelastic analysis of piezoelectric laminae via state space approach. Int. J. Solids Struct. 33, 977–990.

Naillon, M., Coursant, R.H., Besnier, F., 1983. Analysis of piezoelectric structures by a finite element method. Acta Electronica 25, 341–362.

Mitchell, J.A., Reddy, J.N., 1995. A refined hybrid plate theory for composite laminates with piezoelectric laminae. Int. J. Solids Struct. 32, 2345–2367.

Pai, P.F., Nayfeh, A.H., Oh, K., Mook, D.T., 1993. A refined nonlinear model of composite plates with integrated piezoelectric actuators and sensors. Int. J. Solids Struct. 30, 1603–1630.

Peng, X.Q., Lam, K.Y., Liu, G.R., 1998. Active vibration control of composite beams with piezoelectrics: a finite element model with third order theory. J. Sound Vib. 209, 635–650.

Ray, M.C., Rao, K.M., Samanta, B., 1992. Exact solution for static analysis of an intelligent structure under cylindrical bending. Comput. Struct. 47, 1031–1042.

Ray, M.C., Bhattacharya, R., Samanta, B., 1993. Exact solutions for static analysis of intelligent structures. AIAA J. 31, 1684–1691.
Reddy, J.N., 1984. A simple higher order theory for laminated composite plates. J. Appl. Mech. 51, 745–752.
Robbins, D.H., Reddy, J.N., 1991. Analysis of piezoelectrically actuated beams using a layer-wise displacement theory. Comput. Struct. 41, 265–279.
Saravanos, D.A., Heyliger, P.R., 1995. Coupled layerwise analysis of composite beams with embedded piezoelectric sensors and actuators. J. Intell. Mat. Syst. Struct. 6, 350–363.
Saravanos, D.A., Heyliger, P.R., Hopkins, D.A., 1997. Layerwise mechanics and finite element for the dynamic analysis of piezoelectric composite plates. Int. J. Solids Struct. 34, 359–378.
Shu, X., Sun, L., 1994. An improved simple higher-order theory for laminated composite plates. Comput. Struct. 50, 231–236.
Tzou, H.S., 1989. Distributed sensing and controls of flexible plates and shells using distributed piezoelectric element. J. Wave Mater. Interact. 4, 11–29.
Tzou, H.S, Bao, Y., 1995. A theory on anisotropic piezothermoelastic shell laminates with sensor/actuator applications. J. Sound Vib. 184, 453–473.
Xu, K., Noor, A.K., Tang, Y.Y., 1995. Three-dimensional solutions for coupled thermoelectroelastic response of multilayered plates. Comput. Meth. Appl. Mech. Engng. 126, 355–371.
Zhou, H.S., Tiersten, H.F., 1994. Elastic analysis of laminated composite plates in cylindrical bending due to piezoelectric actuators. Smart Mater. Struct. 3, 255–265.